

Applying the Coulomb failure function with an optimally oriented plane to the 2008 Mw 7.9 Wenchuan earthquake triggering

Caijun Xu^{a,*}, Jianjun Wang^a, Zhenhong Li^b, Jane Drummond^b

^a School of Geodesy and Geomatics, Key Laboratory of Geo-space Environment and Geodesy, Ministry of Education, Wuhan University, 129 Luoyu Road, Wuhan, 430079, China

^b Department of Geographical and Earth Sciences University of Glasgow East Quadrangle University Avenue Glasgow G12 8QQ United Kingdom

ARTICLE INFO

Article history:

Received 16 February 2009

Received in revised form 8 September 2009

Accepted 25 September 2009

Available online 4 October 2009

Keywords:

Coulomb stress change

Stress triggering

Optimally oriented plane

Bam earthquake

Wenchuan earthquake

ABSTRACT

The Coulomb failure function (CFF) quantitatively describes static stress changes in secondary faults near the source fault of an earthquake. CFF can be employed to monitor how static stress transfers and then shed some light on the probability of successive events occurring around a source fault. In this paper we focus on the CFF and particularly on optimally oriented planes. We present a unified model to determine an optimally oriented plane and its corresponding Coulomb stress, then apply the model to the 2003 Mw 6.6 Bam (Iran) earthquake and the 2008 Mw 7.9 Wenchuan (China) earthquake, thereby checking its effectiveness. Our results show that spatial correlation between positive Coulomb stress changes and aftershocks are, for the 2003 Bam earthquake, 47.06% when elastic Coulomb stress changes are resolved on uniform planes and 87.53% when these are resolved on optimally oriented planes at depth; for the 2008 Wenchuan earthquake the correlations are 45.68% and 58.20%, respectively. It is recommended that account be taken of optimally oriented planes when drawing a Coulomb stress map for analyzing earthquake triggering effects.

© 2009 Elsevier B.V. All rights reserved.

1. Introduction

The stress state of a fault, or those faults around it, is a crucial indicator of the likelihood that further earthquakes will occur. When critical stress is overcome, a fracture will grow and extend along the direction of least resistance. Therefore, analyzing stress states before and after earthquakes could be helpful in further uncovering the relevant earthquake mechanism and may also shed some light on earthquake prediction. The Coulomb failure function (CFF) is a quantitative description of stress state. To calculate static Coulomb stress, parameters pertaining to the source fault (such as position, length, width, depth, strike, dip and slip vectors) and those pertaining to the receiver fault (such as strike, dip and rake angles) should be determined first. In case studies on earthquake triggering, receiver fault such as strike–slip, dip–slip, or oblique–slip ones have been widely considered (e.g. Reasenber and Simpson, 1992; Harris and Simpson, 1992; King et al., 1994; Harris, 1998; Toda et al., 1998; Toda and Stein, 2000; Tibi et al., 2003; Toda et al., 2005; Ma et al., 2005; Bilek and Bertelloni, 2005; Lin and Stein, 2006; Stein and Lin, 2006; Carli et al., 2008; Console et al., 2008) and for an optimally oriented plane, a receiver fault where maximum Coulomb stress is calculated, with fixed dip and rake angles (e.g. King et al., 1994; Ma et al., 2005; Toda et al., 1998, 2005; Bilek and Bertelloni, 2005). How-

ever, the chosen receiver fault may not always be easy to evaluate. For example, there is uncertainty regarding the receiver fault seismic mechanism of some medium or large earthquakes, thus calculating Coulomb stress is not robust; Or there could be various seismic aftershock mechanisms and thus the selection of a certain receiver fault or optimally oriented plane with limited degrees of freedom may not reflect the real situation; employing an optimally oriented plane with additional degrees of freedom might be more reasonable. Mallman and Zoback (2007) indicated that spatial correlation between Coulomb stress changes and aftershocks could be increased with optimally oriented planes.

In this paper, we present a unified model of Coulomb stress changes on optimally oriented planes. With this unified model, both forward modeling for calculating Coulomb stress changes on given receiver faults and backward modeling for determining Coulomb stress changes on optimally oriented planes can be performed. We slightly extend the previous model pertaining to optimally oriented planes, commonly run on certain kinds of fault planes, for instance, strike–slip planes, to various kinds of planes solely determined by the stress tensor from which Coulomb stress changes are computed. To check its effectiveness, we apply the unified model to analyses of earthquake triggering between the 2003 Mw 6.6 Bam earthquake, the 2008 Mw 7.9 Wenchuan earthquake and their corresponding aftershocks. It is shown that using optimally oriented planes indeed improves the spatial correlation between static Coulomb stress and aftershocks.

* Corresponding author. Tel.: +86 27 68778805; fax: +86 27 68778371.

E-mail address: cjxu@sgg.whu.edu.cn (C. Xu).

2. Optimally oriented plane

The Coulomb failure function (CFF) is defined as (Cocco and Rice, 2002; Steacy et al., 2005a),

$$\Delta CFF = \Delta\tau + \mu(\Delta\sigma_n + \Delta P) \quad (1)$$

where $\Delta\tau$ is the shear stress change along slip on the fault, $\Delta\sigma_n$ is the normal stress change on the fault, ΔP is the pore pressure changes and μ is the friction coefficient.

Assuming $\Delta P = -\beta'\Delta\sigma_{kk}/3$ and $\sigma_{xx} = \sigma_{yy} = \sigma_{zz}$ in the fault zone, we have $\Delta\sigma_{kk}/3 = \Delta\sigma_n$ (Harris, 1998), and then

$$\Delta CFF = \Delta\tau + \mu'\Delta\sigma_n \quad (2)$$

where β' for rock is similar to Skempton's coefficient and $\mu' = \mu(1 - \beta')$.

Now let the stress tensor $\{\sigma^{ij}\}$ be considered in a local topocentric coordinate system whose x , y and z axes are north, east and up respectively. After projecting a stress tensor $\{\sigma^{ij}\}$ along slip on a fault and its normal, one obtains $\Delta\tau$ and $\Delta\sigma_n$. Substituting them into Eq. (2) gives,

$$\begin{aligned} \Delta CFF = & \sin\lambda \left(-\frac{1}{2}\sin^2 A \sin 2\delta\sigma^{11} + \frac{1}{2}\sin 2\delta \sin 2A\sigma^{12} + \cos 2\delta \sin A\sigma^{13} \right. \\ & \left. - \frac{1}{2}\sin 2\delta \cos^2 A\sigma^{22} - \cos 2\delta \cos A\sigma^{23} + \frac{1}{2}\sin 2\delta\sigma^{33} \right) \\ & + \cos\lambda \left(-\frac{1}{2}\sin\delta \sin 2A\sigma^{11} + \sin\delta \cos 2A\sigma^{12} + \cos\delta \cos A\sigma^{13} \right. \\ & \left. + \frac{1}{2}\sin\delta \sin 2A\sigma^{22} + \cos\delta \sin A\sigma^{23} \right) + \mu' (\sin^2\delta \sin^2 A\sigma^{11} \\ & - \sin^2\delta \sin 2A\sigma^{12} - \sin 2\delta \sin A\sigma^{13} + \sin^2\delta \cos^2 A\sigma^{22} \\ & + \sin 2\delta \cos A\sigma^{23} + \cos^2\delta\sigma^{33}) \end{aligned} \quad (3)$$

where A , δ , λ are the strike, dip and rake angles of the receiver fault, and $\{\sigma^{ij} | i, j = 1, 2, 3\}$ are the components of stress tensor induced by earthquake.

Let ΔCFF be a functional $f(\sigma^{ij}, \mu', A, \delta, \lambda)$ and then an optimally oriented plane is such that,

$$\left\{ (A_{\text{opt}}, \delta_{\text{opt}}, \lambda_{\text{opt}}) \mid \max f(\sigma, \mu', A, \delta, \lambda), A \in [0, 2\pi], \delta \in \left[0, \frac{\pi}{2}\right], \lambda \in [-\pi, \pi] \right\} \quad (4)$$

With Eq. (4) an optimally oriented plane can be determined and Coulomb stress changes can be mapped onto it. It is clear in Eq. (4) that an optimally oriented plane is defined as a plane on which the maximum Coulomb stress is found. It is also believed that the occurrence of aftershocks is correlated with positive Coulomb stress. Hence, the spatial correlation between Coulomb stress and aftershocks should be higher on the oriented plane than others. Furthermore, compared with uniform models, the optimally oriented plane has more degrees of freedom on the receiver fault, which may better reflect the real situation. When using optimally oriented planes, it is therefore expected that more reasonable stress maps will be generated for future earthquake hazards.

3. Comparison with previous model

Several previous studies have also considered optimally oriented planes when calculating Coulomb stresses (e.g. King et al., 1994; Toda et al., 1998; McCloskey et al., 2003; Ma et al., 2005; Toda et al., 2005; Bilek and Bertelloni, 2005; Mallman and Zoback, 2007). However, it is only King et al. (1994) who clearly presented formulas of optimally oriented planes in a two-dimensional space. So this section attempts to prove the unified model presented in Section 2 should be identical to those described by King et al. (1994) when the receiver fault has vertical

strike–slips and the stress tensor is a plane stress. In these cases, Eq. (3) can be given as,

$$\begin{aligned} \Delta CFF = & \sin 2A \left[\frac{1}{2}(\sigma^{11} - \sigma^{22}) - \mu'\sigma^{12} \right] \\ & + \cos 2A \left[-\sigma^{12} + \frac{1}{2}\mu'(\sigma^{22} - \sigma^{11}) \right] + \frac{1}{2}\mu'(\sigma^{22} + \sigma^{11}) \end{aligned} \quad (5)$$

for vertical right-lateral strike–slip receiver fault.

The extreme condition is $\frac{\partial(\Delta CFF)}{\partial A} = 0$, that is,

$$\tan 2A = \frac{\frac{1}{2}(\sigma^{11} - \sigma^{22}) - \mu'\sigma^{12}}{\frac{1}{2}\mu'(\sigma^{22} - \sigma^{11}) - \sigma^{12}} \quad (6)$$

With the method of King et al. (1994), that is, the first step is to determine the maximum and minimum principal stresses; the second is to determine the orientation of the receiver fault in the coordinate system whose axes are in fact eigenvectors of stress tensors corresponding to the principal stresses; Finally, the receiver fault plane holds that $A = \frac{\pi}{2} - (\theta + \beta)$, where $\tan 2\theta = \frac{2\sigma^{12}}{\sigma^{22} - \sigma^{11}}$, $\tan 2\beta = \frac{1}{\mu'}$ and thus $\tan 2A = -\frac{\tan 2\theta + \tan 2\beta}{1 - \tan 2\theta \tan 2\beta} = -\frac{2\sigma^{12}\mu' + (\sigma^{22} - \sigma^{11})}{\mu'(\sigma^{22} - \sigma^{11}) - 2\sigma^{12}}$, which is the same as Eq. (6).

Eq. (3) can also be simplified as that,

$$\begin{aligned} \Delta CFF = & \sin 2A \left[\frac{1}{2}(\sigma^{22} - \sigma^{11}) - \mu'\sigma^{12} \right] + \cos 2A \left[\sigma^{12} + \frac{1}{2}\mu'(\sigma^{22} - \sigma^{11}) \right] \\ & + \frac{1}{2}\mu'(\sigma^{11} + \sigma^{22}) \end{aligned} \quad (7)$$

for left-lateral vertical strike–slip receiver fault.

The extreme condition is $\frac{\partial(\Delta CFF)}{\partial A} = 0$, that is,

$$\tan 2A = \frac{\frac{1}{2}(\sigma^{22} - \sigma^{11}) - \mu'\sigma^{12}}{\frac{1}{2}\mu'(\sigma^{22} - \sigma^{11}) + \sigma^{12}} \quad (8)$$

According to the method of King et al. (1994), one obtains $A = \frac{\pi}{2} - (\theta + \beta)$, where $\tan 2\theta = \frac{2\sigma^{12}}{\sigma^{22} - \sigma^{11}}$, $\tan 2\beta = -\frac{1}{\mu'}$ and thus $\tan 2A = -\frac{2\sigma^{12}\mu' - (\sigma^{22} - \sigma^{11})}{\mu'(\sigma^{22} - \sigma^{11}) + 2\sigma^{12}}$, which is the same as Eq. (8).

However, if the fault plane is not a strike–slip or the stress tensor is not a plane stress, an optimally oriented plane should be constrained using Eq. (4). That is the unified model for optimally oriented planes in both two-dimensional and three-dimensional spaces.

4. Application to earthquake triggering

To check the effectiveness of this unified model, we consider two large earthquakes, the 2003 Mw 6.6 Bam (Iran) earthquake and the 2008 Mw 7.9 Wenchuan (China) earthquake. We investigate the spatial correlation between Coulomb stress changes induced by main earthquakes and their aftershocks on given receiver planes and optimally oriented planes. While calculating Coulomb stress changes, the impact of pore pressure due to fluid flow around the fault is usually incorporated into apparent coefficient μ' in Eq. (2) (Harris, 1998). Several apparent coefficients μ' have been considered from 0.0 to 0.8 in order to better explain the relationship between the main shock and its aftershocks (Deng and Sykes, 1997; Parsons et al., 1999; Toda and Stein, 2000; Bilek and Bertelloni, 2005; Parsons et al., 2008). Several studies suggest that aftershocks of thrust faults are sensitive to normal stress changes, implying a relatively high apparent friction coefficient for thrust faults, about 0.8 (Hardebeck et al., 1998; Parsons et al., 1999), while others favor a low friction coefficient for strike–slip faults with a significant cumulative slip, such as the San Andreas, for which it is smaller than 0.4 (Zoback et al., 1987; Harris et al., 1995;

Parsons et al., 1999; Toda and Stein, 2002). Taking account of the Bam earthquake being mainly strike–slip and the Wenchuan earthquake being a significant thrust component in southern sub-fault and a predominantly right-lateral slip in the northern sub-faults, we assume a constant effective friction of $\mu' = 0.4$ for the Bam earthquake and $\mu' = 0.6$ for the Wenchuan earthquake.

4.1. 2003 Mw 6.5 Bam earthquake

The Mw 6.6 Bam earthquake occurred on December 26, 2003 around the city of Bam in the south-east of Iran with the death toll of >26,000, about 30,000 injured and up to 75,000 left homeless (<http://www.reliefweb.int>). A cultural monument nearly intact over the last 2000 years was almost flattened by this earthquake, indicating that it was the largest to occur in this area up till then. Since 1981 four large earthquakes had happened in the Gowk fault zone extending from 50 km west of Bam northward (Wang et al., 2004; Fielding et al., 2005; Talebian et al., 2004). Previous results show that the most seismic moment released along the 20 km long strike–slip shallow fault with a depth of 4–5 km (Talebian et al., 2004; Fialko et al., 2005; Funning et al., 2005). Wang et al. (2004) suggested that the high-precision coseismic deformation data provided by Differential radar interferometry (D-InSAR) could be interpreted with three faulting events and it was the southern segment, a strike–slip with a length of about 13 km, where more than 80 percent of the seismic moment was released and the slip reached a maximum of up to 270 cm. Jackson et al. (2006) had a similar conclusion but the most seismic moment releasing occurred on strike–slip fault of about 15 km length, of up to 2 m slip restricted to the depth range 2–7 km with diverse data source such as synthetic aperture radar, teleseismic seismology, aftershock studies, strong ground motion, geomorphology, remote sensing and surface field work. Such uncertainty of slip distribution on fault arises from date source and strategy of inversion, though some common recognition shows that most seismic moment released at shallow part of crust. We employ the source parameters of the two-segment uniform-slip model presented in Table 3 of Funning et al. (2005) for the source fault. A more precise slip distribution is expected to lead to a more reasonable pattern of the coseismic stress field induced by the earthquake but its general spatial pattern should not dramatically vary (Stacy et al., 2004; Bilek and Bertelloni, 2005).

A three-dimensional Vp, Vs and Poisson's ratio structure in the Bam area using a seismic tomography method and then the general pattern of aftershock distribution was relocated by using the 3-D structure (Sadeghia et al., 2006). It should be noted that the focal mechanisms of the aftershocks remain unknown though such information are required to calculate Coulomb stresses. Hence, an assumption of their focal mechanisms has to be made in this study. As the aim of this study is to derive a unified model from which receiver planes are determined solely by stress tensors induced by earthquake, it is assumed that the aftershocks occurred along a nodal plane where the maximum Coulomb stress changes exist.

Fig. 1 shows the coseismic Coulomb stress fields induced by the 2003 Mw 6.6 Bam earthquake resolved on the receiver faults, parallel to the main fault (a, c) and on optimally oriented planes (b, d). The spatial correlations between Coulomb stress changes and aftershocks on the former receiver faults are not good but are on the latter ones. This indicates that the spatial correlation could be improved when optimally oriented planes are employed. That improvement arises from that fact that more degrees of freedom are allowed for optimally oriented planes and, therefore, Coulomb stress changes on such receiver planes must not be smaller than those on the former ones. This leads to two results: one is to enlarge the zone with positive Coulomb stress changes and the other is to entrench the zones with negative Coulomb stress changes. Accordingly, more aftershocks lie out of the stress shadows and hence the spatial correlation is improved. As shown in Table 1, the triggering rate (i.e. the spatial correlation) in-

creases from 22.17% to 83.47% when Coulomb stress changes are projected onto the optimally oriented planes at depth 5 km, which is consistent with the spatial distribution of aftershocks in the snapshots a and b. It is also the case at depth 10 km, with improvements from 47.06% to 87.53%. Such depth-independent improvement can be theoretically explained by Eq. (4) where only the stress tensor is depth-dependent but an optimally oriented plane still exists for a given stress tensor.

4.2. 2008 Mw 7.9 Wenchuan earthquake

At local time 14:28 (06:28 GMT), on May 12, 2008, a devastating magnitude Mw 7.9 earthquake struck Wenchuan County, Sichuan Province, China, on the eastern edge of the Tibetan Plateau, collapsing myriads of buildings, killing tens of thousands of people and making millions of people homeless. Its epicenter is (30.986°N, 103.364°E) with a depth of 19 km (USGS, 2008). The fault is nearly 270 km long, striking NNE and dipping west, parallel to the northeast-striking Longmen Shan thrust belt (Burchfiel et al., 2008). In the Longmen Shan fault system, going from west to east, sequentially, there are three major faults: the Wenchuan-Maowen fault; the Beichuan-Yingxiu fault and the Pengxian-Guanxian fault. Pre-existing documents show that none of these faults were obviously active, e.g., the rate of thrusting being less than 1.1 mm/a and the rate of strike-slipping being less than 1.46 mm/a (Zhou et al., 2007); ~3 mm/year right-slip and ~2 mm/year convergence along the Longmen Shan boundary (Meade, 2007). This tectonic zone was so quiescent that few paid much attention to it except for a limited number of research group, e.g. Densmore et al. (2007).

Ji and Hayes (2008) quickly determined the slip distribution of this large event using broadband waveforms and suggested that of the best fitted nodal plane was (strike = 229°, dip = 33°). The slip distribution shows that most of the seismic moments released at depth 6–18 km, the largest slip is about 9 meters lying between two clusters and the reverse and right-slip components are of comparable magnitude along the southwestern portion, while right-slip dominates the northern portion. Recently, Li et al. (2008) employed seven adjacent pairs of ascending JAXA's ALOS PALSAR images and three independent pairs of descending ESA's ENVISAT ASAR images to determine fault trace and then invert a variable slips with four-segment sub-faults. They reported that the average slips in the northern sub-faults were smaller than those in the southern one. The latter had a significant thrust component whilst the other segments had a predominantly right-lateral slip. We use their four-segment dislocation model as the mechanism of the source fault, since it can recover more than 95% of the observed deformation signals (Li et al., 2008).

Fig. 2 shows the static Coulomb stress changes resolved on receiver faults parallel to the average mechanism of the 2008 Wenchuan earthquake (a, c) and on optimally oriented planes (b, d) at depth 5 km and 10 km respectively. Similar to the case of the 2003 Bam earthquake, employing optimally oriented planes can improve the spatial correlation between Coulomb stress changes and aftershocks. As shown in Table 2, at depth 5 km the triggering rate (i.e. the spatial correlation) is improved from 31.68% to 44.10%; and, at depth 10 km from 45.68% to 58.20%. Fig. 3 is the same as Fig. 2 but at depths 15 km and 20 km. The triggering rate is improved from 54.72% to 66.95% at depth 15 km; and, at depth 20 km from 56.81% to 67.70%.

Fig. 4 shows the static Coulomb stress changes resolved on receiver faults parallel to the average mechanism of the 2008 Wenchuan earthquake (a, c) and on optimally oriented planes (b, d) at depth 10 km with dislocation models from Ji and Hayes (2008) (a, b) and from Sladen (2008) (c, d). This shows that improvements in the spatial correlation between Coulomb stress changes and aftershocks also can be obtained by employing optimally oriented planes. Quantitatively, Table 3 shows that the triggering rate is improved

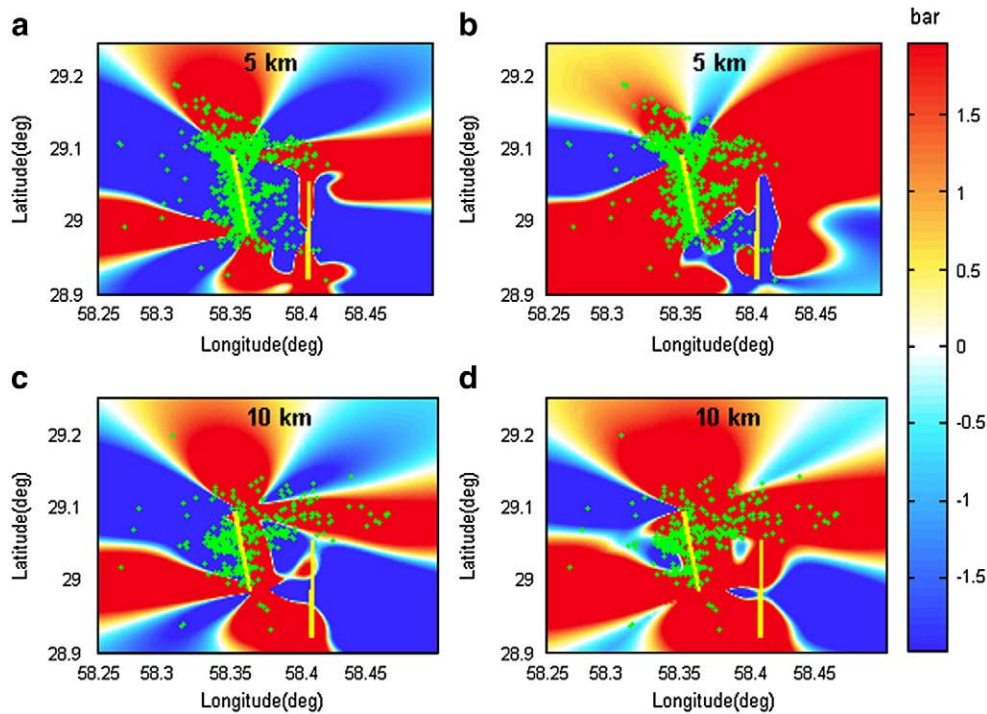


Fig. 1. Static Coulomb stress changes induced by 2003 Mw 6.5 Bam earthquake and resolved on receiver faults parallel to main fault (a and c) and on optimally oriented planes (b and d) at depth 5 km and 10 km respectively. Black dots represent all the aftershocks with magnitudes ranging from 0.1 to 3.1 during the period from 2004/2/8 to 2004/3/6 (Sadeghia et al., 2006). Aftershocks at each snapshot are from bins of the depth range of $h \pm 2.5$ km where h is the corresponding depth of that snapshot. Black thick lines are the projections of upper edges of fault planes at surface.

from 31.67% to 43.18% for Ji and Hayes's dislocation model and from 40.30% to 76.10% for Sladen's model. But, it seems that limitations exist to improving the triggering rate of aftershocks when employing optimally oriented planes, which is discussed next.

5. Discussion

5.1. Optimally oriented plane: robustness

As shown in Eq. (4), Coulomb stress change on an optimally oriented plane is a function of stress tensor. Accordingly, any mechanism of imparting stress tensor to nearby secondary fault must effect Coulomb stress changes on optimally oriented plane, for instance, coseismic dislocation, interseismic accumulation and postseismic effects.

Coseismic dislocation of earthquake faults makes two kinds of stress changes, one is static stress change and the other is dynamic stress change. The former is time-independent because it is born from net slippage on a fault, whilst the latter is time-dependent because it arises from the shaking of instantaneous seismic waves. However they cannot be distinguished from each other over short times and distances from the hypocenter (Steady et al., 2005a). Interseismic strain accumulation by creeping on some fault segments also perturbs the stress state in the vicinity of earthquake fault (Biggs et al., 2007). Postseismic effects such as: postseismic relaxation coming from lower crust and upper mantle

Table 1

Triggering rate of aftershocks of 2003 Mw 6.5 Bam earthquake with magnitude range from 0.1 to 3.1 during time 2004/2/8–2004/3/6 at different depth levels (Sadeghia et al., 2006).

Depth	Receiver fault	Triggering rate
5 km	Parallel to source fault	22.17%
	Optimally oriented plane	83.47%
10 km	Parallel to source fault	47.06%
	Optimally oriented plane	87.53%

(Freed and Lin, 2001; To et al., 2004; Pollitz et al., 2006); afterslip along fault planes in the shallower or deeper depths of the crust; and, pore-elastic rebound due to fluid flow in rocks (Peltzer et al., 1996; Jonsson et al., 2003), also makes contribution to the stress state around fault. Taking account of these mechanisms from which alternate stress and strain can be derived, and those stress tensors which are a priori information constraining an optimally oriented plane, a full picture of stress tensors should be drawn before calculating Coulomb stress.

Secondly, the mathematical dislocation model of those mechanisms referred to above should be carefully investigated because they are used to determine stress tensors, as is necessary during calculating Coulomb stress changes. As for those such as coseismic dislocation and postseismic relaxation, some favor Okada's uniform half-space model (e.g. King et al., 1994; Toda and Stein, 2000; Tibi et al., 2003; Steacy et al., 2004; McCloskey et al., 2005; Bilek and Bertelloni, 2005; Nalbant et al., 2005; Stein and Lin, 2006), while others Pollitz's spherical layered model (e.g. Freed et al., 2007; Pollitz and Schwartz, 2008), finite element model (e.g. Deng and Sykes, 1997; Freed and Lin, 2001). Differences of calculated stress tensor born from different dislocation models should be considered.

Thirdly, a major source error for calculating Coulomb stress changes comes from the uncertainties of the parameters of receiver fault planes where stress changes are projected. Some previous studies did calculation on the fault planes (e.g. Reasenber and Simpson, 1992; McCloskey et al., 2005; Parsons et al., 2008), whilst others employed the rupture directions of the aftershocks in their calculation (e.g. Toda and Stein, 2000; Freed et al., 2007; Chen et al., 2008). The former focused on stress triggering between earthquake faults and the latter paid attention to stress triggering between the main shock and its aftershocks. As there is usually no information on the focal mechanisms of aftershocks but their hypocenters, the uncertainties of receiver faults keep existing and which receiver fault to be selected in the calculation remains an open question.

Figs. 2a,c and 4a,c show Coulomb stress changes resolved on a receiver fault parallel to the average mechanism of a source fault.

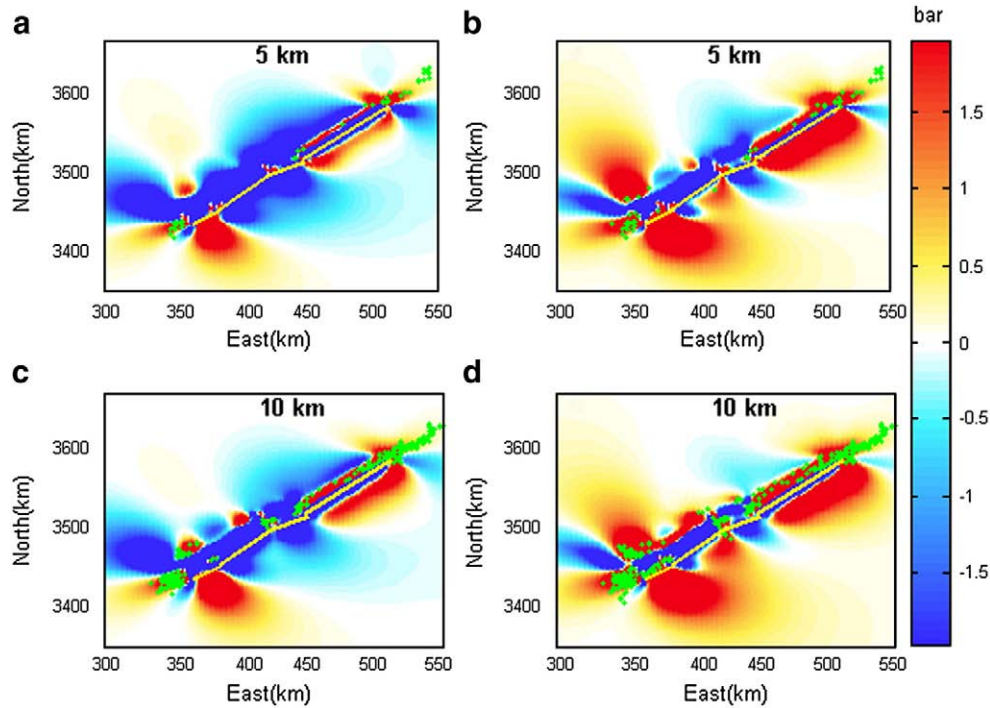


Fig. 2. Static Coulomb stress changes resolved on receiver faults parallel to the average mechanism of the 2008 Wenchuan earthquake source faults (a and c) and on optimally oriented planes (b and d) at depth 5 km and 10 km respectively. Black dots represent those aftershocks lying in the zones of positive Coulomb stress from the 2883 aftershocks with magnitudes ranging from 2.0 to 6.5 during the period from 12 May to 8 July 2008 (Huang et al., 2008) for clearer comparison among snapshots. Aftershocks at each snapshot are from bins of the depth range of $h \pm 2.5$ km where h is the corresponding depth of that snapshot. White thick lines are the projections of upper edges of fault planes at surface.

Aftershock distributions are equally poorly explained by Coulomb stress changes, for instance, triggering rates are 45.68%, 31.67% and 40.30% sequentially in Table 3. However, if an optimally oriented plane is considered, triggering rates can be improved to be 58.20%, 43.18% and 76.10% respectively (Table 3).

To sum up, to obtain a robust optimally oriented plane, the stress tensor of a Coulomb stress function should be treated carefully from three aspects: one is the mechanism driving stress transfer in an earthquake cycle; another is the dislocation model depicting such a driving mechanism; the third is the choice of receiver fault plane.

5.2. Optimally oriented plane: effectiveness and limitation

Optimally oriented planes belong to the set of receiver fault planes and are sometimes determined solely by the stress tensor imparted by the source fault but other times incorporate tectonic stress (e.g. King et al., 1994; Steacy et al., 2005b; Mallman and Zoback, 2007). Compared with determining an optimally oriented plane, determining a general receiver fault is direct if seismological and geological information show parameters of the targeted fault. It is not direct if it is required

to observe the spatial-temporal evolution of aftershocks, because most of them are small magnitude and their focal mechanisms cannot be definitely determined. In this case, some workers assume that the focal mechanisms of the aftershocks are the same as those of the main earthquake (e.g. King et al., 1994; Steacy et al., 2004; Freed et al., 2007), or the average strike of the main earthquakes (e.g. Toda and Stein, 2000), or optimally oriented thrust fault planes (e.g. Bilek and Bertelloni, 2005), or a smooth interpolation between mapped faults (e.g. Toda et al., 2008). Though most can explain the spatial pattern of aftershocks very well, which of those assumptions is valid is still an open question. As far as optimally oriented plane is concerned, Coulomb stress change resolved on such a plane is the upper bound of sets of all ones resolved on possible planes; not surprising to improve the spatial correlation between Coulomb stress and aftershocks (Figs. 1b, d, 2b, 2d, 3b, 3d, 4b and 4d). However, whether aftershocks rupture along such planes, or not, is still to be verified. Some think so, but no consensus has been obtained. For instance, McCloskey et al. (2003) stated that aftershock failure planes were constrained by geological structure, but not poorly determined regional stress, and proposed that geological structure should be combined with the philosophy of an optimally oriented plane. In other words, the optimally oriented planes came from the set of observed possible failure planes. Steacy et al. (2005b) showed that stress maps best fitting the observed aftershock distributions generally could be produced if regional stress is well constrained, whereas if regional stress is poorly constrained or the tectonic environment is complex, the best model might be to fix the strike of the planes but allow the dip and rake to vary. Mallman and Zoback (2007) reported that estimating the Coulomb stress changes on optimally oriented planes in three dimensions rather than two dimensions improved correlation between Coulomb stress changes and rate increases.

Another important issue is the overestimation of the triggering rate for an optimally oriented plane. The optimally oriented plane is none other than the one on which the maximum Coulomb stress exists and therefore overestimation of Coulomb stress might be unavoidable.

Table 2

Triggering rate of aftershocks of 2008 Mw 7.9 Wenchuan earthquake with magnitude range from 2.0 to 6.5 during the period from 2008/5/12 to 2008/7/8 (Huang et al., 2008) at different depth levels for the dislocation model of Li et al. (2008).

Depth	Receiver fault	Triggering rate
5 km	Parallel to source fault	31.68%
	Optimally oriented plane	44.10%
10 km	Parallel to source fault	45.68%
	Optimally oriented plane	58.20%
15 km	Parallel to source fault	54.72%
	Optimally oriented plane	66.95%
20 km	Parallel to source fault	56.81%
	Optimally oriented plane	67.70%

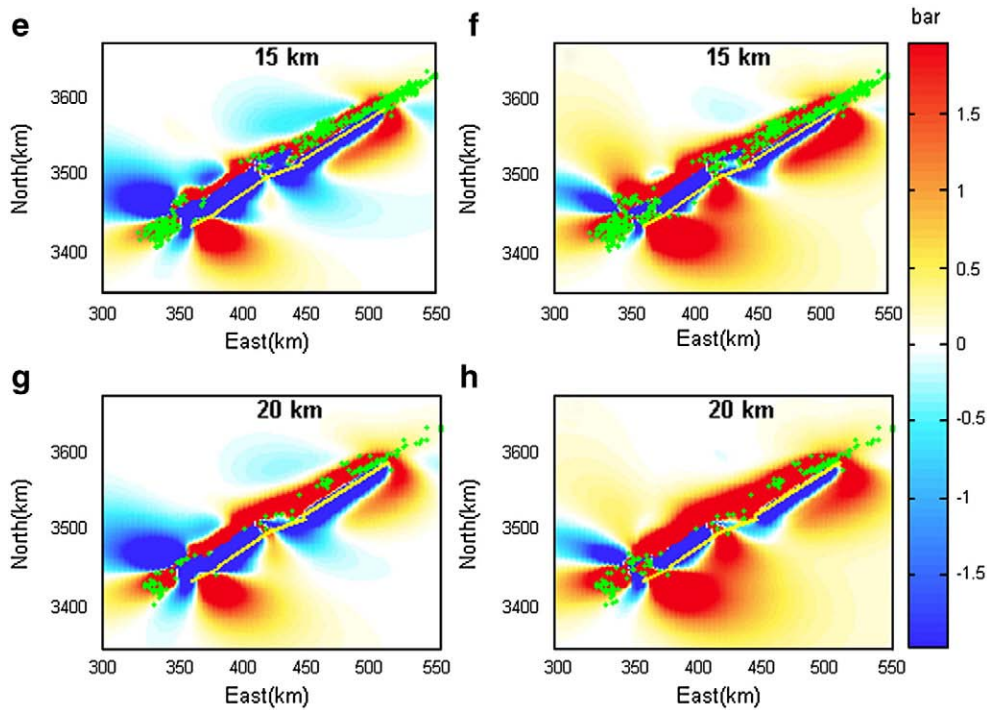


Fig. 3. Static Coulomb stress changes resolved on receiver faults parallel to the average mechanism of the 2008 Wenchuan earthquake source faults (e and g) and on optimally oriented planes (f and h) at depth 15 km and 20 km respectively. Black dots represent the those aftershocks lying in the zones of positive Coulomb stress from the 2883 aftershocks with magnitudes ranging from 2.0 to 6.5 during the period from 12 May to 8 July 2008 (Huang et al., 2008) for clearer comparison among snapshots. Aftershocks at each snapshot are from bins of the depth range of $h \pm 2.5$ km where h is the corresponding depth of that snapshot. White thick lines are the projections of upper edges of fault planes at surface.

When employing optimally oriented planes, one should take care of this point. Besides, it seems that there is a limitation of the model pertaining to optimally oriented planes for interpreting the triggering effect between the main earthquake and its aftershocks from case studies on

the two large earthquakes considered above. We propose that it may be simplistic to just consider coseismic stress tensor, but postseismic, dynamic and tectonic stresses are indeed ignored in the Coulomb stress model.

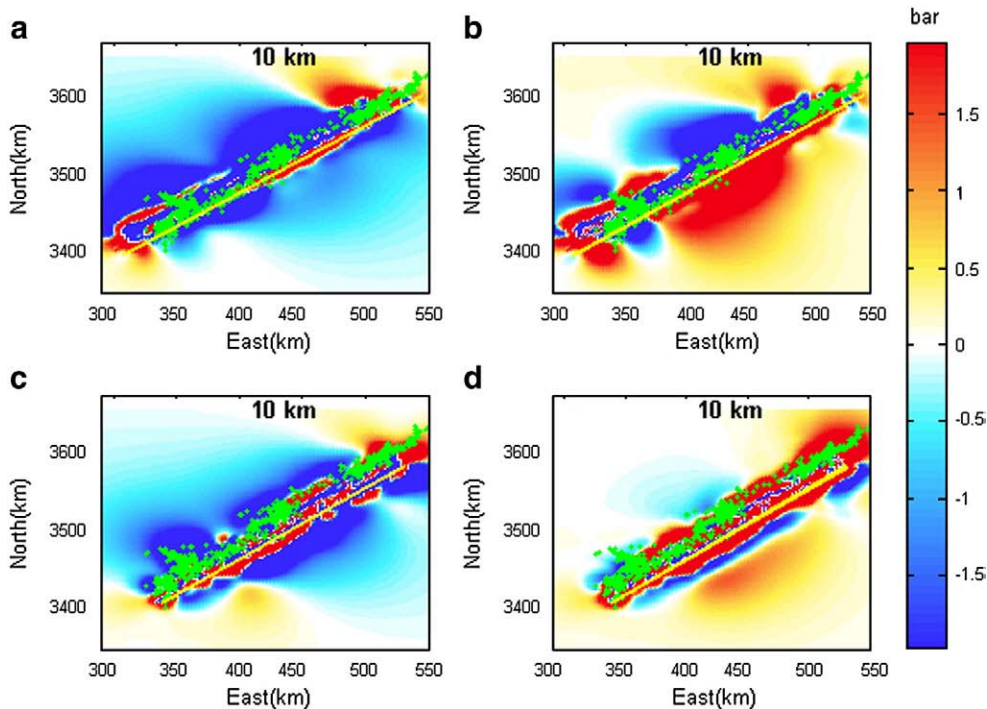


Fig. 4. Static Coulomb stress changes on receiver planes parallel to the average mechanism of the 2008 Wenchuan earthquake source fault (a and c) and on optimally oriented planes (b and d) at depth 10 km. Dislocation models of source fault are from Ji and Hayes (2008) (a and b) and Sladen (2008) (c and d). White dots represent those 2883 aftershocks with magnitudes ranging from 2.0 to 6.5 during the period from 12 May to 8 July 2008 (Huang et al., 2008). Aftershocks at each snapshot are from bins of the depth range of $h \pm 2.5$ km where h is the corresponding depth of that snapshot. Black thick lines are the projections of upper edges of fault planes at surface.

Table 3

Triggering rate of aftershocks of 2008 Mw 7.9 Wenchuan earthquake with magnitude range from 2.0 to 6.5 during the period from 2008/5/12 to 2008/7/8 (Huang et al., 2008) at depth 10 km for different dislocation models.

Source fault	Receiver fault	Triggering rate
Li et al. (2008)	Parallel to source fault	45.68%
	Optimally oriented plane	58.20%
Ji and Hayes (2008)	Parallel to source fault	31.67%
	Optimally oriented plane	43.18%
Sladen (2008)	Parallel to source fault	40.30%
	Optimally oriented plane	76.10%

6. Conclusions

In this paper we present a model to calculate Coulomb stress changes on an optimally oriented plane. We apply this model to the 2003 Mw 6.6 Bam earthquake and to the 2008 Mw 7.9 Wenchuan earthquake to investigate the spatial correlation between Coulomb stress changes and aftershocks. We suggest that the use of optimally oriented planes can significantly improve spatial correlation compared to the use of uniform planes. This is because the intrinsic nature of the model of the three-dimensional optimally oriented planes increases the degrees of freedom on the receiver planes. One can derive static Coulomb stress changes with the unified model, draw an initial stress map and then refine it with a more precise slip distribution to make better static stress map, which could be significant in earthquake prediction.

Acknowledgements

This work was supported by a grant from the National Natural Science Foundation of China (no. 40874003 and no. 40721001), the National High Technology Research and Development Program of China (863 Program) (no. 2009AA12Z317), the National Department Public Benefit Research Foundation (Earthquake) (no. 200808080), and the Program of Introducing Talents of Discipline to Universities (no. B07037). We are grateful to Dr Hossein Sadeghi for making available relocated aftershock data at Bam and Dr Yuan Huang for providing relocated aftershock data for the Wenchuan event.

References

Biggs, J., Wright, T., Lu, Z., Parsons, B., 2007. Multi-interferogram method for measuring interseismic deformation: Denali Fault, Alaska. *Geophys. J. Int.* 170, 1165–1179. doi:10.1111/j.1365-246X.2007.03415.x.

Bilek, S.L., Bertelloni, C.L., 2005. Stress changes in the Costa Rica subduction zone due to the 1999 Mw = 6.9 Quepos earthquake. *Earth Planet. Sci. Lett.* 230, 97–112.

Burchfiel, B.C., Royden, L.H., Van der Hilst, R.D., et al., 2008. A geological and geophysical context for the Wenchuan earthquake of 12 May 2008, Sichuan, People's Republic of China. *Geol. Soc. Am. Today* 18 (7). doi:10.1029/2007JB004951.

Carli, S.D., Voisin, C., Cotton, F., Semmane, F., 2008. The 2000 western Tottori (Japan) earthquake: triggering of the largest aftershocks and constraints on the slip-weakening distance. *J. Geophys. Res.* 113, B05307. doi:10.1029/2007JB004951.

Chen, K.H., Toda, S., Rau, R., 2008. A leaping, triggered sequence along a segmented fault: the 1951 ML 7.3 Hualien-Taitung earthquake sequence in eastern Taiwan. *J. Geophys. Res.* 113, B02304. doi:10.1029/2007JB005048.

Cocco, M., Rice, J.R., 2002. Pore pressure and poroelasticity effects in Coulomb stress analysis of earthquake interactions. *J. Geophys. Res.* 107 (B2). doi:10.1029/2000JB000138.

Console, R., Murru, M., Falcone, G., Catalli, F., 2008. Stress interaction effect on the occurrence probability of characteristic earthquakes in Central Apennines. *J. Geophys. Res.* 113, B08313. doi:10.1029/2007JB005418.

Deng, J., Sykes, L.R., 1997. Evolution of the stress field in southern California and triggering of moderate-size earthquakes: a 200-year perspective. *J. Geophys. Res.* 102 (9859), 9886.

Densmore, A.L., Ellis, M.A., Li, Y., Zhou, R., Hancock, G.S., Richardson, N., 2007. Active tectonics of the Beichuan and Pengguan faults at the eastern margin of the Tibetan Plateau. *Tectonics* 26, TC4005. doi:10.1029/2006TC001987.

Fialko, Y., Sandwell, D., Simons, M., Rosen, P., 2005. Three-dimensional deformation caused by the Bam, Iran, earthquake and the origin of shallow slip deficit. *Nature* 435, 295–299. doi:10.1038/nature03425.

Fielding, E.J., Talebian, M., Rosen, P.A., Nazari, H., Jackson, J.A., Ghorashi, M., Walker, R., 2005. Surface ruptures and building damage of the 2003 Bam, Iran, earthquake mapped by satellite synthetic aperture radar interferometric correlation. *J. Geophys. Res.* 110, B03302. doi:10.1029/2004JB003299.

Freed, A.M., Lin, J., 2001. Delayed triggering of the 1999 Hector Mine earthquake by viscoelastic stress transfer. *Nature* 411, 180–183.

Freed, A.M., Ali, S.T., Burgmann, R., 2007. Evolution of stress in Southern California for the past 200 years from coseismic, postseismic and interseismic stress changes. *Geophys. J. Int.* 169, 1164–1179. doi:10.1111/j.1365-246X.2007.03391.x.

Funning, G.J., Parsons, B., Wright, T.J., 2005. Surface displacements and source parameters of the 2003 Bam (Iran) earthquake from Envisat advanced synthetic aperture radar imagery. *J. Geophys. Res.* 110, B09406. doi:10.1029/2004JB003338.

Hardebeck, J., Nazareth, J., Hauksson, E., 1998. The static stress change triggering mode: constraints from two southern California aftershock sequences. *J. Geophys. Res.* 103, 24,427–24,437.

Harris, R.A., 1998. Introduction to special section: Stress triggers, stress shadows, and implication for seismic hazard. *J. Geophys. Res.* 103, 24,347–24,358.

Harris, R.A., Simpson, R.W., 1992. Changes in static stress on southern California faults after the 1992 Landers earthquake. *Nature* 360, 251–254.

Harris, R.A., Simpson, R.W., Reasenberg, P.A., 1995. Influence of static stress changes on earthquake locations in southern California. *Nature* 375, 221–224.

Huang, Y., Wu, J., Zhang, T., Zhang, D., 2008. Relocation of the M 8.0 Wenchuan earthquake and its aftershock sequence. *Sci. China* 51, 1703–1711.

Jackson, J., Bouchon, M., Fielding, E., et al., 2006. Seismotectonic, rupture process, and earthquake-hazard aspects of the 2003 December 26 Bam, Iran, earthquake. *Geophys. J. Int.* 166, 1270–1292.

Jonsson, S., Segall, S., Pedersen, R., Bjornsson, G., 2003. Post-earthquake ground movements correlated to pore-pressure transients. *Nature* 424, 179–183.

Ji, C., and Hayes G., 2008. Preliminary result of the May 12, 2008 Mw 7.9 eastern Sichuan, China earthquake, http://earthquake.usgs.gov/eqcenter/eqinthenews/2008/us2008ryan/finite_fault.php.

King, G.C.P., Stein, R.S., Lin, J., 1994. Static stress changes and the triggering of earthquakes. *Bull. Seismol. Soc. Am.* 84, 935–953.

Li Z., E. Fielding J., Wright T., Parsons B., and Feng W., 2008. Fault trace and slip in the 2008 Mw 7.9 Sichuan, China earthquake from InSAR and GPS observations, AGU Fall Meeting 2008 Eos Trans. AGU, 89(53), Fall Meet. Suppl., Abstract G33C-0714.

Lin J., and Stein R.S., 2006. Seismic constraints and Coulomb stress changes of a blind thrust fault system, 1: Coalinga and Kettleman Hills, California, Open-File Report 2006-1149.

Ma, K.F., Chan, C., Stein, R.S., 2005. Response of seismicity to Coulomb stress triggers and shadows of the 1999 Mw = 7.6 Chi-Chi, Taiwan, earthquake. *J. Geophys. Res.* 110, B05S19. doi:10.1029/2004JB003389.

Mallman, E.P., Zoback, M.D., 2007. Assessing elastic Coulomb stress transfer models using seismicity rates in southern California and southwestern Japan. *J. Geophys. Res.* 112, B03304. doi:10.1029/2005JB004076.

McCloskey, J., Nalbant, S.S., Steacy, S., 2005. Earthquake risk from co-seismic stress. *Nature* 434, 291.

McCloskey, J., Nalbant, S.S., Steacy, S.S., Nostro, C., Scotti, O., Baumont, D., 2003. Structural constraints on the spatial distribution of aftershocks. *Geophys. Res. Lett.* 30 (12), 1610. doi:10.1029/2003GL017225.

Meade, B.J., 2007. Present-day kinematics at the India–Asia collision zone. *Geology* 35, 81–84. doi:10.1130/G22924A.1.

Nalbant, S.S., Steacy, S., McCloskey, J., 2005. Stress transfer relations among the earthquake that occurred in Kerman province, Southern Iran since 1981. *Geophys. J. Int.* 167, 309–318.

Parsons, T., Stein, R.S., Simpson, R., Reasenberg, P., 1999. Stress sensitivity of fault seismicity: a comparison between limited-offset oblique and major strike-slip faults. *J. Geophys. Res.* 104, 20,183–20,202.

Parsons, T., Chen, J., Kirby, E., 2008. Stress changes from the 2008 Wenchuan earthquake and increased hazard in the Sichuan basin. *Nature* 454, 509–510. doi:10.1038/nature07177.

Peltzer, G., Rosen, P., Rogenz, F., Hudnut, K., 1996. Postseismic rebound in fault step-overs caused by pore fluid flow. *Science* 273 (5279), 1202–1204.

Pollitz, F.F., Banerjee, P., Burgmann, R., Hashimoto, M., Choosakul, N., 2006. Stress changes along the Sunda trench following the 26 December 2004 Sumatra-Andaman and 28 March 2005 Nias earthquakes. *Geophys. Res. Lett.* 33, L06309. doi:10.1029/2005gl024558.

Pollitz, F.F., Schwartz, D.P., 2008. Probabilistic seismic hazard in the San Francisco Bay area based on simplified viscoelastic cycle model of fault interactions. *J. Geophys. Res.* 113, B05409. doi:10.1029/2007JB005227.

Reasenberg, P.A., Simpson, R.W., 1992. Response of regional seismicity to the static stress change produced by the Loma Prieta earthquake. *Science* 255, 1687–1690.

Sadeghia, H., Aghda, S.M.F., Suzuki, S., Nakamura, T., 2006. 3-D velocity structure of the 2003 Bam earthquake area (SE Iran): existence of a low-Poisson's ratio layer and its relation to heavy damage. *Tectonophysics* 417, 269–283.

Sladen, A., 2008. http://www.tectonics.caltech.edu/slip_history/2008_e_sichuan/e_sichuan.html.

Steacy, S., Marsan, D., Nalbant, S.S., McCloskey, J., 2004. Sensitivity of static stress calculations to the earthquake slip distribution. *J. Geophys. Res.* 109, 4303.

Steacy, S., Gombert, J., Cocco, M., 2005a. Introduction to special section: stress transfer, earthquake triggering and time-dependent seismic hazard. *J. Geophys. Res.* 110, B05S01. doi:10.1029/2005JB003692.

Steacy, S.S., Nalbant, S., McCloskey, J., 2005b. Onto what planes should Coulomb stress perturbations be resolved? *J. Geophys. Res.* 110, B05S15. doi:10.1029/2004JB003356.

Stein, S.S. and J. Lin (2006). Seismic constraints and Coulomb stress changes of a blind thrust fault system, 2: Northridge, California, Open-File Report 2006-1158.

Talebian, M., et al., 2004. The 2003 Bam (Iran) earthquake: rupture of blind strike-slip fault. *Geophys. Res. Lett.* 31, L11611. doi:10.1029/2004GL020058.

Tibi, R., Wiens, D.A., Inoue, H., 2003. Remote triggering of deep earthquakes in the 2002 Tonga sequences. *Nature* 424, 921–925.

To, A., Burgmann, R., Pollitz, F., 2004. Postseismic deformation and stress changes following the 1891 Rann of Kachchh, India earthquake: was the 2001 Bhuj earthquake a triggered event? *Geophys. Res. Lett.* 31, L13609. doi:10.1029/2004GL020220.

- Toda, S., Stein, R.S., Reasenber, P.A., Dieterich, J.H., Yoshida, A., 1998. Stress transferred by the 1995 Mw = 6.9 Kobe, Japan, shock: effect on aftershocks and future earthquake probabilities. *J. Geophys. Res.* 103, 24,543–24,565.
- Toda, S., Stein, R.S., 2000. Did stress triggering cause the large off-fault aftershock of the 25 March 1998 Mw = 8.1 Antarctic plate earthquake? *Geophys.Res.Lettts.* 27 (15), 2301–2304.
- Toda, S., Stein, R.S., 2002. Response of the San Andreas fault to the 1983 Coalinga-Nunez earthquakes: an application of interaction-based probabilities for Parkfield. *J. Geophys. Res.* 107 (B6), 2126. doi:10.1029/2001JB000172.
- Toda, S., Stein, R.S., Dinger, K.R., Bozkurt, S.B., 2005. Forecasting the evolution of seismicity in southern California: animations built on earthquake stress transfer. *J. Geophys. Res.* 110, B05S16. doi:10.1029/2004JB003415.
- Toda, S., Lin, J., Meghraoui, M., Stein, R.S., 2008. 12 May 2008 M = 7.9 Wenchuan, China, earthquake calculated to increase failure stress and seismicity rate on three major fault systems. *Geophys. Res. Lett.* 35, L17305. doi:10.1029/2008GL034903.
- USGS, 2008. <http://earthquake.usgs.gov/eqcenter/eqinthenews/2008/us2008ryan/>.
- Wang, R., Xia, Y., Grosse, H., Wetzel, H.-U., Kaufmann, H., Zschau, J., 2004. The 2003 Bam (SE Iran) earthquake: precise source parameters from satellite radar interferometry. *Geophys. J. Int.* 159, 917–922.
- Zoback, M.D., et al., 1987. New evidence on the state of stress of the San Andreas fault system. *Science* 238, 1105–1111.
- Zhou, R., Li, Y., Densmore, A.L., Ellis, M.A., He, Y., Li, Y., Li, X., 2007. Active tectonics of the Longmen Shan region of the eastern margin of the Tibetan plateau. *Acta Geol. Sin.* 81, 593–604.